Polymer 51 (2010) 3736–3743

Contents lists available at ScienceDirect

Polymer

journal homepage: www.elsevier.com/locate/polymer

High efficient UV-A photodetectors based on monodispersed ligand-capped TiO_2 nanocrystals and polyfluorene hybrids

Yangang Han, Gang Wu*, Mang Wang, Hongzheng Chen

MOE Key Laboratory of Macromolecule Synthesis and Functionalization, State Key Laboratory of Silicon Materials, Department of Polymer Science and Engineering, Zhejiang University, Hangzhou 310027, PR China

ARTICLE INFO

Article history:
Received 26 February 2010
Received in revised form
4 May 2010
Accepted 28 May 2010
Available online 9 June 2010

Keywords:
Optical–electronic materials
Polymer composite materials
Photodetectors

ABSTRACT

Monodispersed ligand-capped TiO_2 nanocrystals are synthesized by a low temperature solvothermal method using oleic acid (OA) as the capping agent. The single layer hybrid films based on the OA-capped TiO_2 nanocrystals and poly(9,9-dihexylfluorene) (PFH) are prepared by solution processing at room temperature and characterized by atomic force microscopy, UV–vis absorption and photoluminescence spectra. The hybrid film is applied in the fabrication of nanostructured UV-A photodetector (320–420 nm) by sandwiching it between two electrodes to form bulk heterojunction. The high ultraviolet signal-to-noise ratio of 3 orders of magnitude with short response time less than 200 ms can be achieved for the device. Furthermore, the device shows drastic changes in current under a wide range of UV irradiation with a linear relationship between them. The thermal behavior of the device is also discussed. The high photosensitivity in the UV-A range and the low-cost endow them with potential for environmental and biological uses.

1. Introduction

In recent years, ultraviolet (UV) photodetectors have drawn much attention for their civil and military uses such as solar UV monitoring, flame sensors, UV communication, space research, and so on [1–3]. According to the common classification of UV light with respect to the wavelength, only the longest wavelength of the UV-A range (320–420 nm) can reach the Earth's surface. The UV-B light (280–320 nm) and the UV-C light (200–280 nm) can be completely absorbed by the molecules in sunscreen lotions and the molecules in the Earth's atmosphere, respectively, not allowing them to reach the ground [4]. Since the UV-A light may cause some diseases such as a skin cancer, developing novel UV-A photodetectors with high sensitivity to the UV-A light becomes more and more important.

Most of the UV-A detectors are made of inorganic semiconductors such as doped GaN [5], ZnO [6], and TiO_2 [7,8] due to their wide bandgap, fast response time, higher response, and stability. However, they are constructed on expensive substrates such as sapphire, and the related fabrications are troublesome and costly, which limit their large-scale applications. Besides the inorganic systems, organic UV-A detectors have undergone rapid development recently. Compared to their inorganic counterparts, organic photodetectors are considered as a complementary for the advantages of simple fabrication processes, lighter weight and lower cost [9]. Their performance, however, is worse than the inorganic ones [10]. However, Lin et al. reported organic UV photodetectors consisting of large bandgap triaryldiamine and oxadiazole-containing oligoaryls as the efficient electron-transfer donor–acceptor couple, which have comparable efficiencies to a commercial UV-A photodetector made of GaN and cover the whole UV-A range [11]. Compared with the pure inorganic or organic devices, the organic/inorganic hybrid devices, combining the advantages of each component and overcoming their disadvantages, usually indicate obvious superiority [12–14]. UV-A detectors applying poly(9,9-dihexylfluorene) (PFH) and ZnO nanorods arrays were recently reported by Lin et al. [15]. Yamaura et al. [16] fabricated PEDOT:PSS (poly(3,4-ethylenedioxythiophene)-poly (styrenesulfonate))/$SrTiO_3$:Nb hybrid UV photodiode which is only activated in the UV region and exhibits a large response to the UV-B light. The studies on the organic/inorganic hybrid UV-A photodetectors are still not too much.

In this work, we have developed a UV-A hybrid detector based on a *p-n* junction consisting of *n*-type TiO_2 nanocrystals and *p*-type polymer PFH. The active hybrid layer of the device is prepared by spin-coating of the polymer solution mixed with ligand-capped TiO_2 nanocrystals. PFH has a large bandgap and strong absorption in UV-A range, which could be used as the donor and hole-

* Corresponding author. Tel.: +86 571 87953733; fax: +86 571 87953733.
E-mail addresses: wmang@zju.edu.cn (G. Wu), hzchen@zju.edu.cn (H. Chen).

0032-3861/$ – see front matter © 2010 Elsevier Ltd. All rights reserved.
doi:10.1016/j.polymer.2010.05.057

transporting material. TiO_2 nanocrystals act as the acceptor and electron-transporting material. It has been found that high quality TiO_2 nanocrystals with good crystallinity and a narrow size distribution are very important for well-tailored chemicophysical properties [17]. And applications of the hybrids in the optoelectronic devices rely on the dispersion of the inorganic nanocrystals in the polymer matrix in order to create a high interfacial surface area for excitons diffusion to the interface and separation into free carriers [18,19]. In this work, the ligand (Oleic acid (OA)) used could fulfill all the requirements mentioned above. Furthermore, it is much cheaper compared with other commonly used ligands such as linoleic acid [20] and does not need a high reaction temperature to fabricate TiO_2 nanocrystals.

2. Experimental

2.1. Synthesis and characterization of monodispersed ligand-capped TiO_2 nanocrystals

Ligand-capped TiO_2 nanocrystals were synthesized using a solvothermal method. OA was used as the ligand. OA (63.5 mL), triethylamine (12.5 mL), NH_4HCO_3 (2.5 g), and cyclohexane (12.5 mL) were mixed at room temperature. Then 2.5 mL of Ti $(OBu)_4$ was added dropwise into the mixed solution. After stirring for 10 min, the solution was transferred into a 100 mL Teflon-lined autoclave and heated at 180 °C for 20 h. When cooled to room temperature, the crude product was precipitated with an excess of ethanol and washed with ethanol two times to remove the surfactant residuals. The final product was then dispersed in chloroform for further study.

X-ray diffraction measurement (XRD, RIGAKU D/MAX 2550/PC) with monochromatic Cu Kα radiation was carried out to examine the crystal structure of the particles. The morphology was studied by transmission electron microscope (TEM, JEOL JEM-200 CX). Particle size was determined by a particle size analyzer (90Plus/BI-MAS Multi Angle Particle Sizing Option, Brookhaven Instruments Corporation).

2.2. Fabrication and characterization of TiO_2 nanocrystals/PFH hybrids

In the preparation of hybrid films, the polymer PFH solution (2.5 mg/mL) was prepared by dissolving PFH (Mw = 24 000, PDI = 2.4, purchased from Beijing Synwit Technology Co. Ltd.) in chloroform. Hybrid dispersions with different contents of OA-capped TiO_2 nanocrystals were obtained by mixing the required amount of TiO_2 dispersion with PFH solution. Hybrid thin films were prepared by spin-coating the hybrid dispersion on the substrates for further use. The nanostructure was investigated by atomic force microscopy (AFM, Veeco Instruments Inc.) using tapping mode. Optical properties of the hybrid films were studied via UV–vis absorption measurements (Varian Cary100) and photoluminescence measurements (Perkin–Elmer LS55).

2.3. Device fabrication and characterization

The hybrid photosensitive layer (60 nm) made up of TiO_2 and PFH was spin-coated onto the PEDOT:PSS (40 nm) pre-coated ITO bottom electrode, followed by evaporation of a 40 nm thick Al electrode under vacuum. The effective cell area was adjusted to about 0.075 cm^2. The current–voltage (I–V) characteristic and photoresponse of the device were recorded with a Keithley 236 source-measure unit under the excitation of a high pressure mercury lamp (CHG-200) equipped with a 365 nm bandpass filter. For spectral response measurement, a 500 W Xenon lamp and a grating monochromator were used. The measurements were conducted at room temperature in the air. To study the influence of annealing on the device performance, the as-prepared device was heated at 90 °C (the glass transition temperature of PFH is about 80 °C) in vacuum for variable duration.

3. Results and discussion

3.1. Morphology of monodispersed OA-capped TiO_2 nanocrystals and their hybrid films with PFH

Ligand-capped TiO_2 nanocrystals were synthesized at 180 °C using OA as the ligand. As shown in Fig. 1a, the typical peaks owing to the (101), (004), (200), (211), and (213) reflections of the anatase phase are found at $2\theta = 25.3$, 37.8, 48.0, 54.0, and 62.7°, indicating that OA-capped TiO_2 nanocrystal powder is characteristic of bulk anatase TiO_2 with a high degree of crystallinity [21]. The particles' morphology is illustrated in the TEM image in Fig. 1b, from which the mean particle diameter is about 8–10 nm and no aggregates of TiO_2 nanocrystals are found with the help of the organic ligand [22]. The particle size distribution measured by a particle size analyzer was summarized in the inset of Fig. 1b. It is obvious that monodispersed nanocrystals have been obtained. The calculated average particle size is 10.5 nm, which is similar to that obtained from the TEM image.

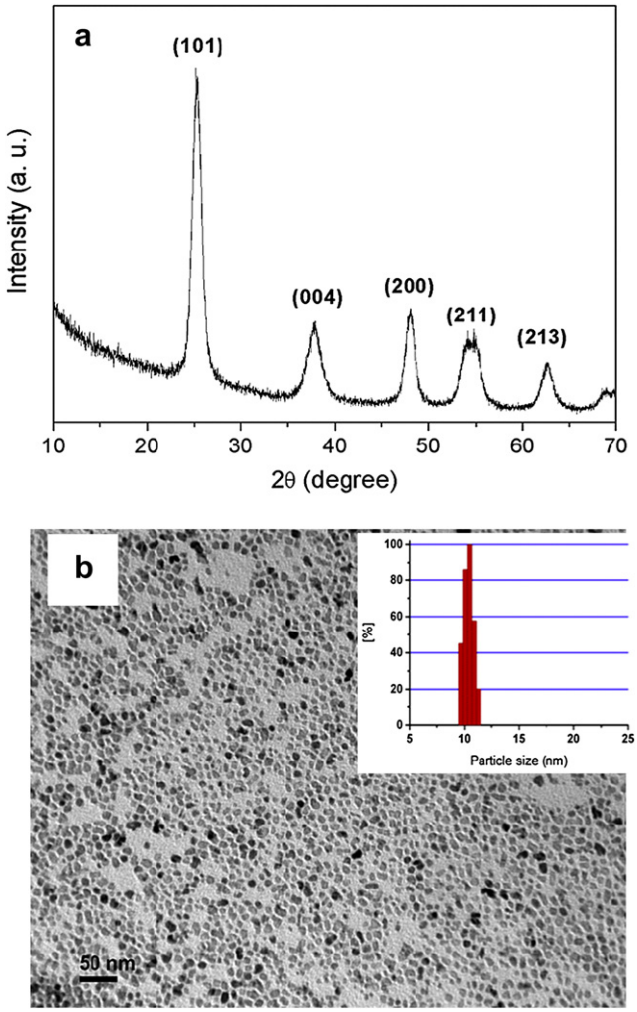

Fig. 1. XRD pattern (a) and TEM image (b) of the as-prepared OA-capped TiO_2 nanocrystals. The inset is the particle size distribution of the OA-capped TiO_2 nanocrystals.

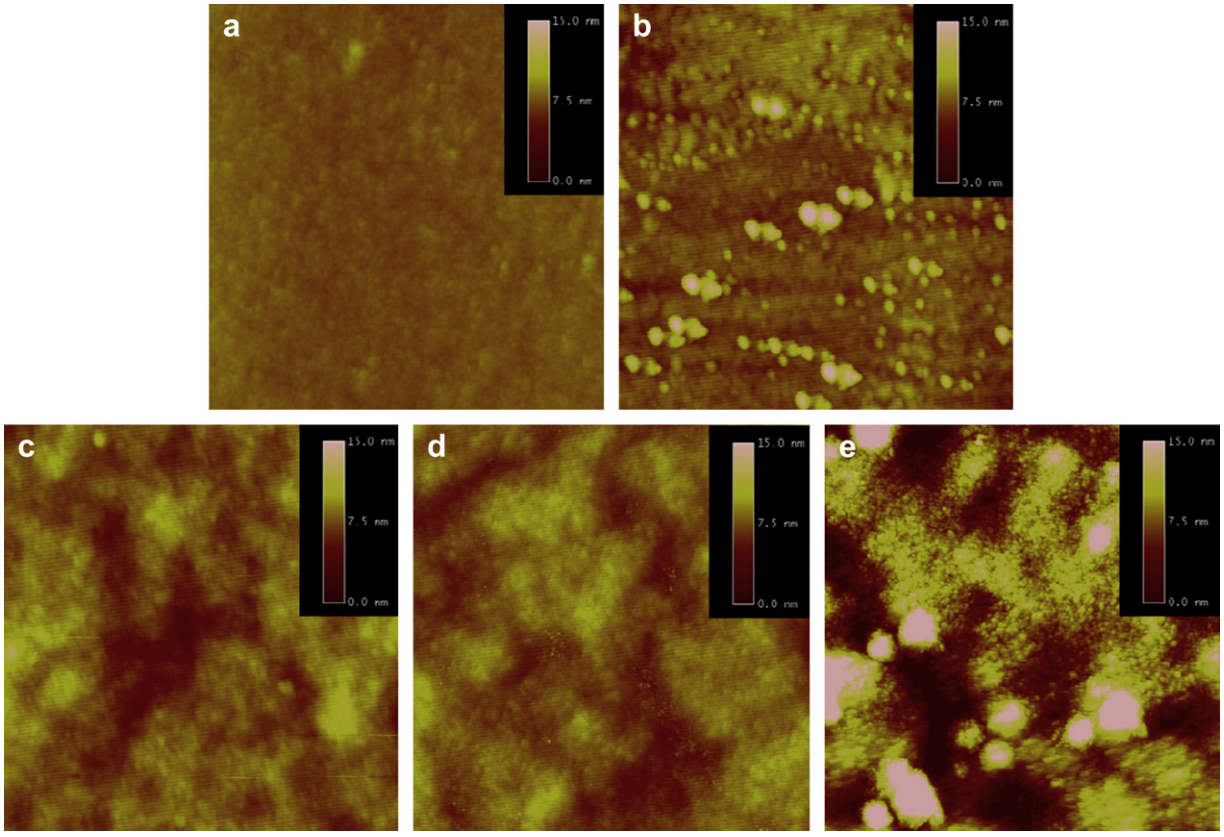

Fig. 2. AFM topography images of TiO_2 nanocrystals/PFH hybrid films consisting of 0, 10, 30, 50, and 70 wt% TiO_2 nanocrystals. The scanning range is 2 μm × 2 μm. (a) 0 wt%, $r_{RMS} = 0.88$ nm, (b) 10 wt%, $r_{RMS} = 1.33$ nm, (c) 30 wt%, $r_{RMS} = 1.19$ nm, (d) 50 wt%, $r_{RMS} = 1.22$ nm, and (e) 70 wt%, $r_{RMS} = 4.10$ nm.

Fig. 2(a–e) presents the AFM images of the hybrid films with different contents of TiO_2 nanocrystals. For the pristine PFH film, the surface is very smooth with a root mean square roughness (r_{RMS}) of 0.88 nm. When the TiO_2 content increases to 10 wt%, the TiO_2 nanocrystals are dispersed in the polymer matrix with an r_{RMS} of 1.33 nm. For the films containing 30 and 50 wt% TiO_2, the polymer and TiO_2 nanocrystals are well mixed to achieve bi-continuous pathways in the whole layer for efficient charge separation [23], showing r_{RMS} values of 1.19 and 1.22 nm, respectively. Fig. 2e clearly shows that the addition of the excess TiO_2 nanocrystals (70 wt%) greatly increases the roughness of the film (r_{RMS} of 4.10 nm) with a large agglomerate formation.

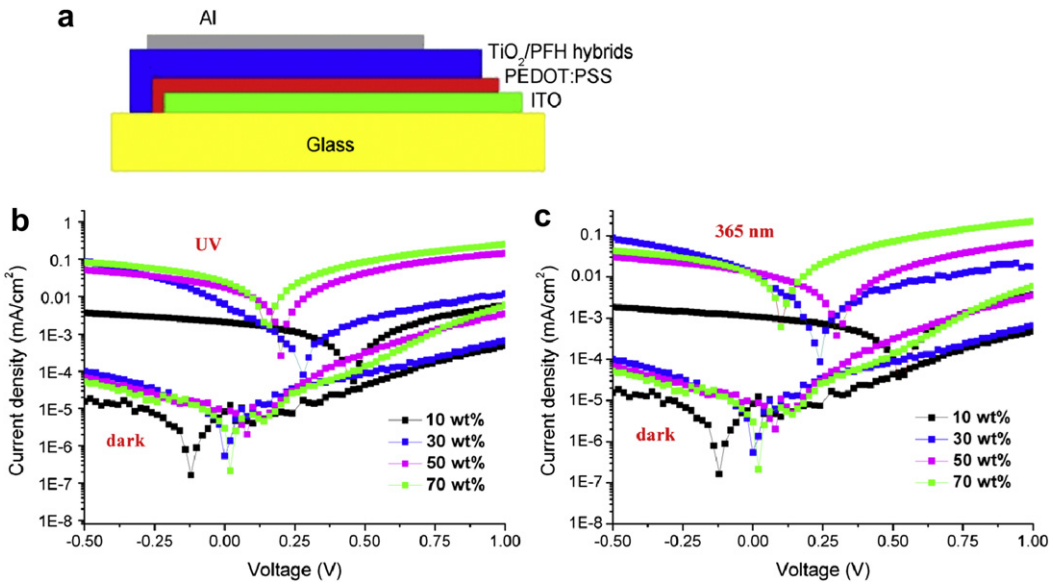

Fig. 3. (a) Schematic representation of the photovoltaic devices based on the hybrid materials (ITO/PEDOT:PSS/TiO_2-PFH hybrids/Al). Current-voltage characteristics for the TiO_2 nanocrystals/PFH hybrid devices consisting of 10, 30, 50, and 70 wt% TiO_2 nanocrystals under 3.2 mW/cm^2 UV irradiation by using a high pressure mercury lamp (b) and 0.7 mW/cm^2 irradiation at 365 nm (c).

3.2. Performance of TiO_2 nanocrystals/PFH hybrid devices

A schematic diagram of our standard device configuration, consisting of a transparent ITO conducting electrode, PEDOT:PSS layer, the TiO_2 nanocrystals/PFH hybrid layer, and an aluminum electrode, is shown in Fig. 3a. The I–V curves for the four devices with different TiO_2 contents from 10, 30, 50 and 70 wt% under UV illumination and in dark are shown in Fig. 3b and c. Two types of UV light sources are used. One is the light from the high pressure mercury lamp (named as UV) and the other is from the same lamp equipped with a 365 nm bandpass filter (named as 365 nm). Obvious photovoltaic effects are observed in all devices. The open-circuit voltage (V_{OC}) decreases and the current density increases gradually with the increased content of TiO_2 under either UV or 365 nm illumination. The current density increases with the reverse bias, which is due to the enhanced separation efficiency of geminate charge pairs proved from the PL spectra and the improved extraction efficiency of the separated carriers from electrodes at higher electric fields [11].

PL quenching in the TiO_2 nanocrystals/PFH hybrid is a useful indication of the degree of exciton dissociation. When irradiated under light of 380 nm, only the polymer is excited and the PL spectra of the hybrids show similar emission features to that of the pristine PFH, indicating that the luminescence predominantly results from the excitons radiatively recombined in polymer [24]. It can be found in Fig. 4 that with the content increase of TiO_2 nanocrystals, a significant PL quenching has occurred. For the hybrid consisting of 50 wt% TiO_2 nanocrystals, the quenching efficiency exceeds 55%, suggesting the occurrence of exciton dissociation at the interface between TiO_2 nanocrystals and PFH.

The time dependence measurements of photoresponse were employed to investigate the rise and decay speed of the photocurrent upon switching UV light on and off. As shown in Fig. 5a, the current increases rapidly to a certain level upon switching on UV light, then recovers to the original value when the light source is removed. The photocurrent densities of the hybrids containing 10, 30, 50, and 70 wt% TiO_2 at zero bias are 1.94, 19.0, 15.5, and 13.0 μA/cm^2, respectively. The photocurrent of the high TiO_2 loading (30, 50, 70 wt%) hybrids is obviously larger than that (1.94 μA/cm^2) of the low loading (10 wt%) system. For the high concentration devices, the photocurrent however decreases with increasing the TiO_2 loading from 30 to 70 wt%. This phenomenon can be ascribed to the reduced interfacial area between the two components because of the agglomeration of TiO_2 nanoparticles. The dark current of the devices with different TiO_2 contents does not change much (about 0.02 μA/cm^2). The ultraviolet signal-to-noise ratio of the hybrids can reach as high as 3 orders of magnitude except the 10 wt% device (2 orders of magnitude). The rise time for each of the four devices is shorter than 200 ms, which is the detecting limit of our equipments. And the photocurrent remains stable under the persistent irradiation. However, the decay time is quite different. For the device containing 50 wt% TiO_2, the current is restored to dark status within 1.5 s after the removal of the light source. As to the device containing 70 wt% TiO_2, the decay time is around 5 s. The fast rise and decay could be attributed to the solid-state process in which electron–hole pairs are generated instantaneously by UV light and recombination of photogenerated electron–hole pairs [25]. The periodic process shown in Fig. 5 can be steadily repeated for more than 500 times. We also examined the device containing pure PFH and found that the photocurrent density at zero bias is less than 1 μA/cm^2. Furthermore, the response time is much longer (more than 15 s) than the hybrid device and could not recover to the original value in a short time. Similar phenomenon is found when the 365 nm UV light source is applied (Fig. 5b). Only a little decrease of ultraviolet signal-to-noise ratio (near 3 orders of magnitude) can be found because of the peak absorption of the hybrids located at 370 nm other than 365 nm. The high ultraviolet signal-to-noise ratio, fast response and good reproducibility endow the hybrids potential applications in the field of UV light switches and detectors.

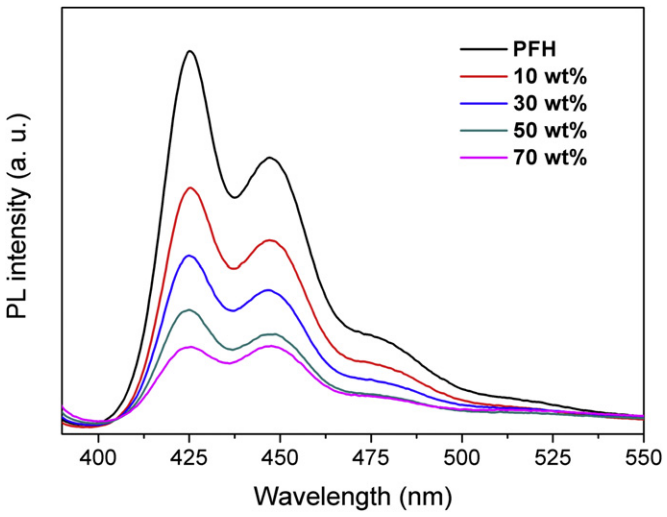

Fig. 4. Photoluminescence spectra of the TiO_2 nanocrystals/PFH hybrid films consisting of 0, 10, 30, 50, and 70 wt% TiO_2 nanocrystals, excited at 380 nm.

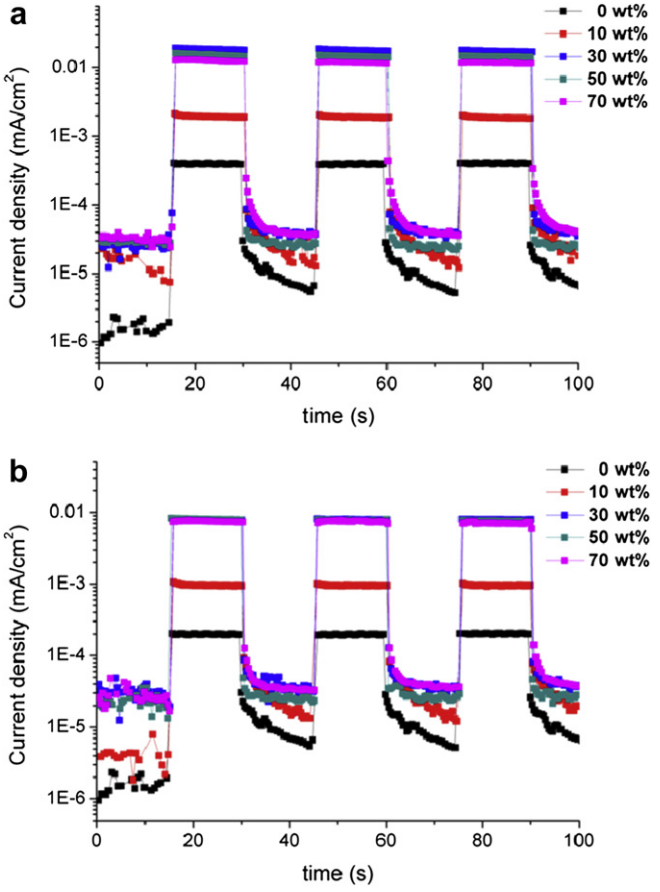

Fig. 5. Time dependence of the photocurrent rise and decay under periodic illumination of (a) 3.2 mW/cm^2 UV irradiation and (b) 0.7 mW/cm^2 365 nm UV light. The bias is 0 V.

The I–V characteristics of the hybrid device containing 50 wt% TiO_2 nanocrystals under various intensities of UV irradiation are shown in Fig. 6a and b. Under either UV irradiation or 365 nm UV light, the photocurrent increases with increased intensity of the UV light. As shown in Fig. 6c and d, the current of the device could be reversibly modulated by UV irradiation. The response time and the recovery time under any intensity of UV irradiation in the experimental range are as short as 200 ms. The linear relationship between photocurrent and irradiation intensity can be found in Fig. 6e and f. This means that there is no significant buildup of space charge, which can cause deviation from linear dependence of light intensity [26]. The sensitivity of the device, which is determined by the slope of the correlation curve between photocurrent and irradiation intensity, is 2.94 mA/W under UV irradiation and 6.92 mA/W under 365 nm UV light. Obviously, the device is more sensitive to the 365 nm UV light than the UV irradiation, which is consistent with the photoresponse spectra presented in the following text. Such a device can give different signal in quantity under different UV intensity, and can be applied to measure the intensity of the UV irradiation directly.

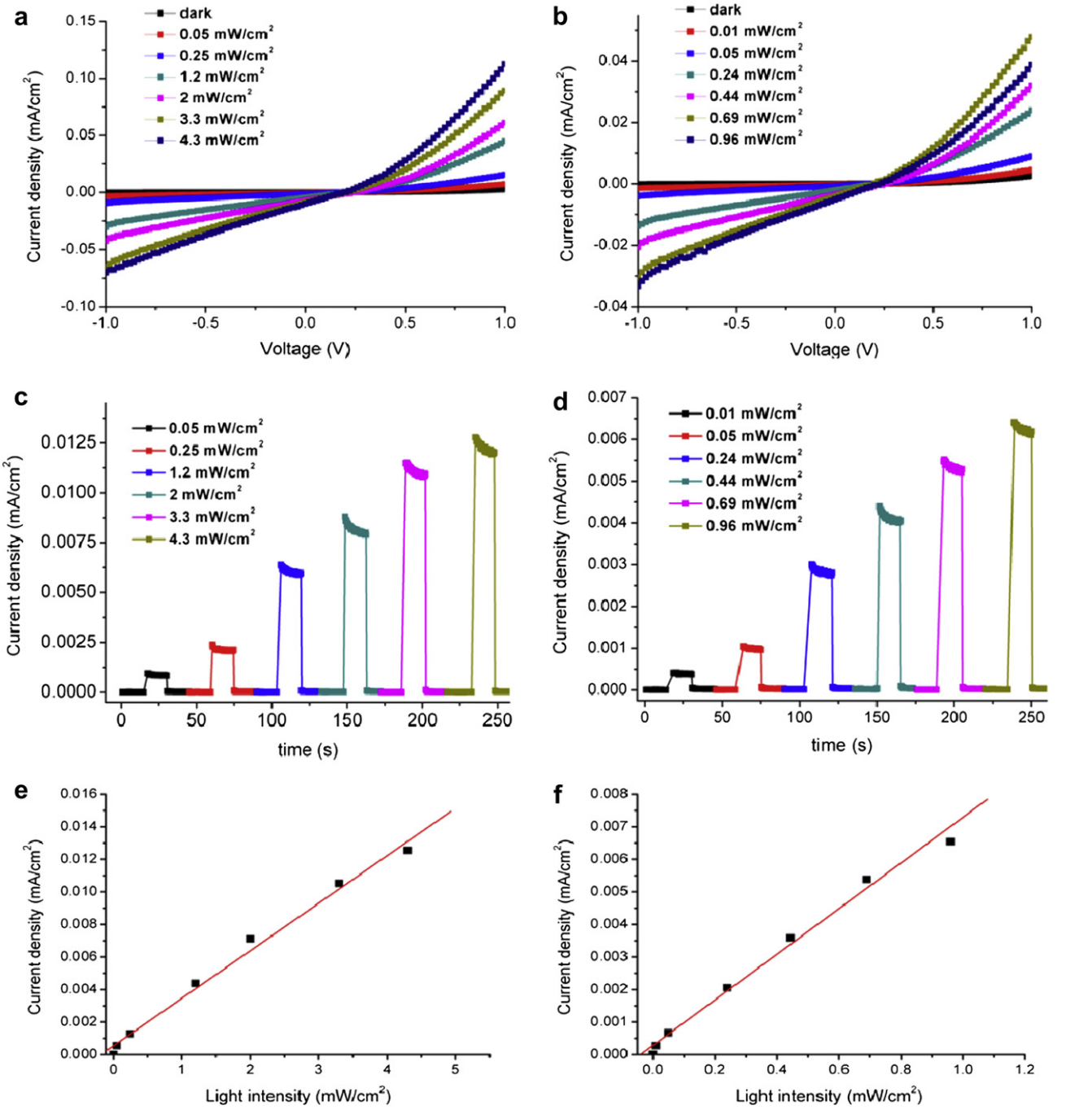

Fig. 6. The current–voltage curves of the hybrid device containing 50 wt% TiO_2 nanocrystals under (a) UV irradiation and (b) 365 nm light with different intensities. Time dependence of the 50 wt% device under periodic illumination of (c) UV light and (d) 365 nm light at zero bias. The current measured at zero bias as a function of the UV light (e) and 365 nm light (f), respectively. The red lines are the linear fits of the data. For interpretation of the references to colour in this figure legend, the reader is referred to the web version of this article.

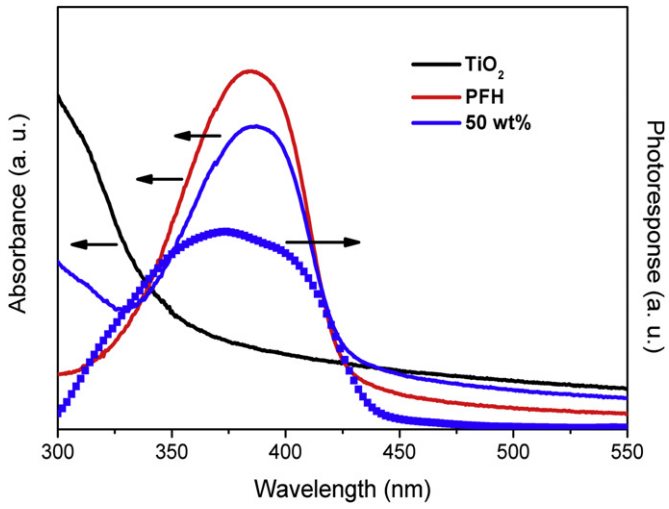

Fig. 7. Photoresponse and absorption spectra as a function of wavelength of incident light for the hybrid film containing 50 wt% TiO_2 nanocrystals.

The spectral response and the optical absorption of the device are compared. The wavelength dependence of the photocurrent of the hybrid device containing 50 wt% TiO_2 is shown in Fig. 7. The absorption of the hybrid is the simple superposition of the absorption spectra of the constituents. The spectral response, however, is quite different. The peak located at 300 nm corresponding to the absorption of TiO_2 disappears, revealing that light absorbed by the polymer contributes mostly to the photosensitivity. This phenomenon is also found in P3HT/TiO_2 system [27]. Under optical excitation, excitons are formed in the donor molecules of the hybrid layer, which is the polymer PFH in this case. When an exciton in a donor molecule approaches an acceptor molecule in the hybrid layer, it can be dissociated and the resulted charge carriers transfer to the corresponding electrodes.

3.3. Influence of annealing

Thermal annealing is the most common way to improve the solar cell efficiency [28–30]. However, the annealing effect on the polymer based on fluorene is still not clear. Therefore, we further investigated the effect of annealing on the nanoscale morphology as well as the corresponding device performance.

Fig. 8 shows the annealing-time dependence of the UV sensitivity for the hybrid devices containing 50 wt% TiO_2 nanocrystals. The device was annealed at 90 °C which is 10 °C above the glass transition temperature of PFH. Meanwhile, there is no structural change to OA at this temperature. It can be seen from Fig. 8a that the photocurrent decreases with increasing the annealing time

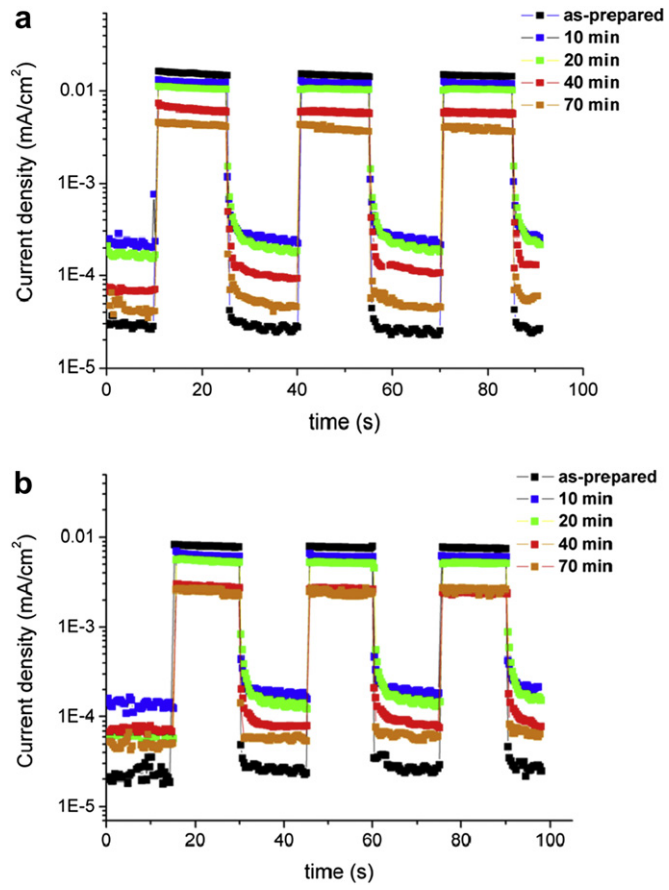

Fig. 8. Time dependence of the annealed hybrid devices containing 50 wt% TiO_2 nanocrystals under periodic illumination of (a) 3.2 mW/cm^2 UV irradiation and (b) 0.7 mW/cm^2 365 nm light at zero bias.

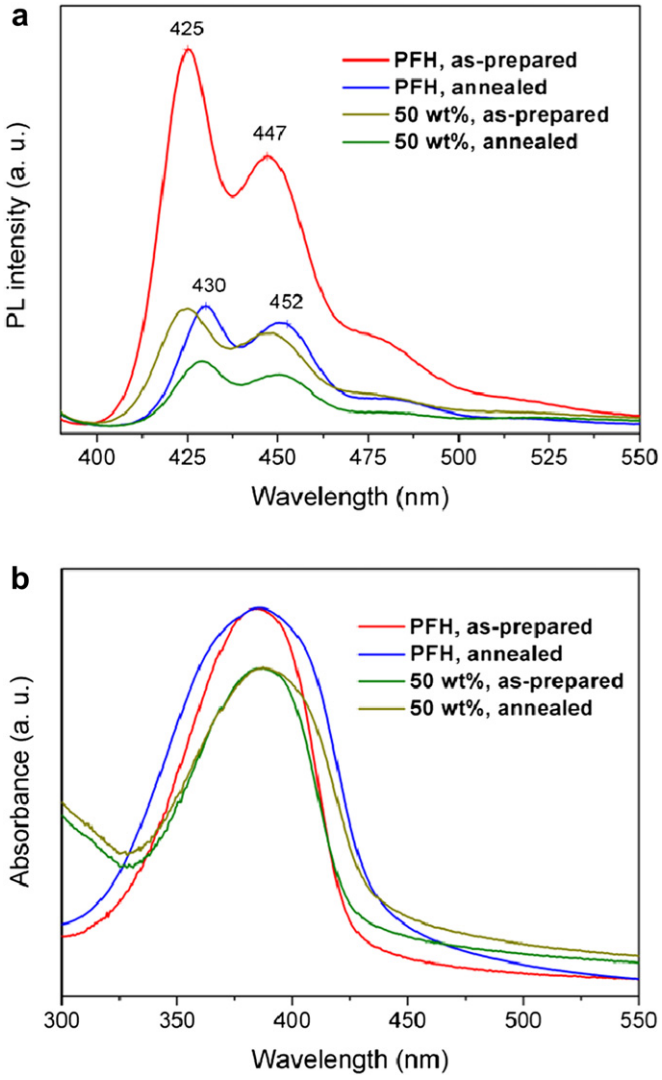

Fig. 9. Photoluminescence (a) and UV–vis absorption (b) spectra of the as-prepared hybrid film containing 50 wt% TiO_2 nanocrystals and the annealed film (90 °C for 40 min).

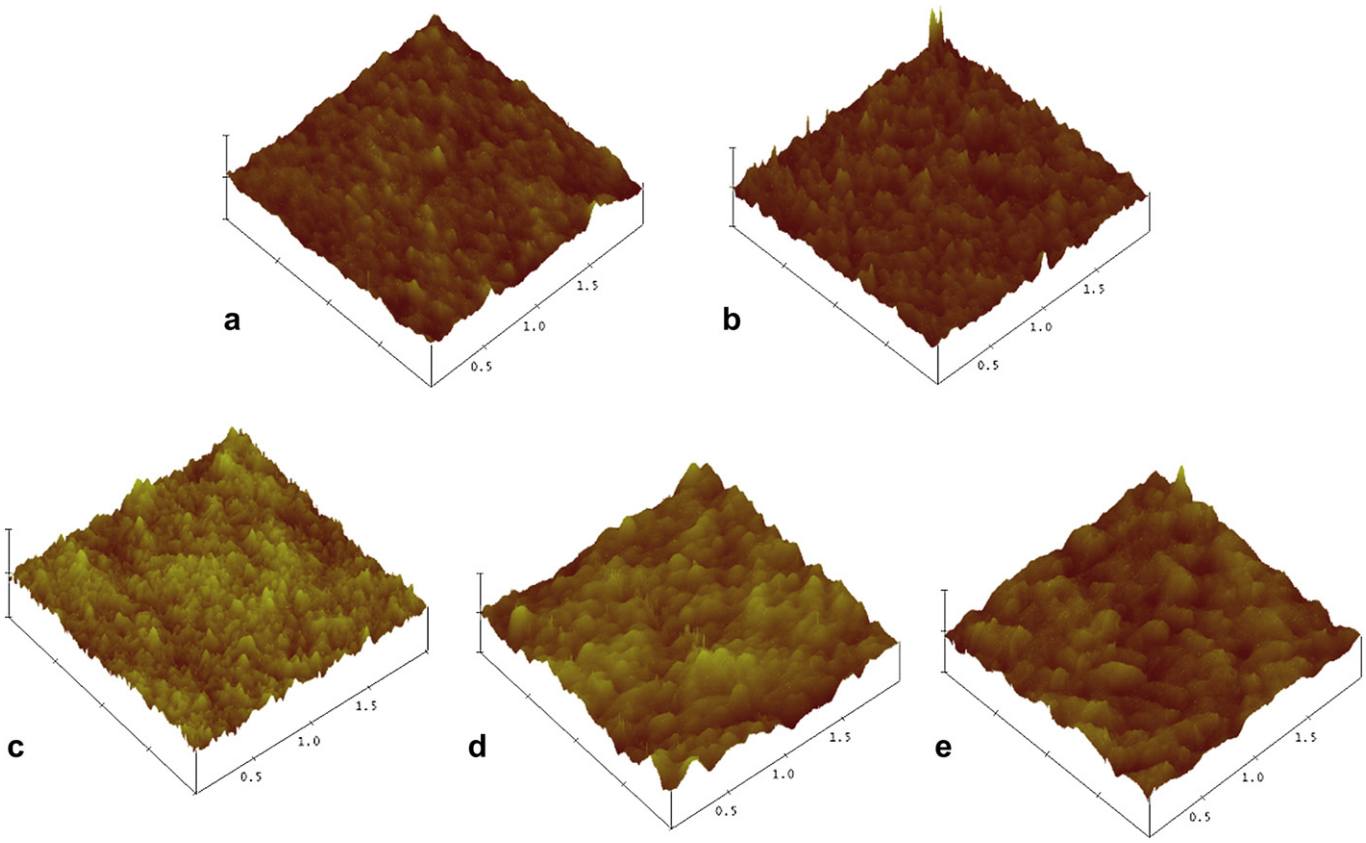

Fig. 10. 3-D topography images taken from the hybrid films containing 50 wt% TiO_2 nanocrystals after annealing at 90 °C for various time. (a) as-prepared film, $r_{RMS} = 1.22$ nm, (b) 10 min, $r_{RMS} = 1.24$ nm, (c) 20 min, $r_{RMS} = 1.27$ nm, (d) 40 min, $r_{RMS} = 1.52$ nm, and (e) 70 min, $r_{RMS} = 1.81$ nm. The scanning range is 2 μm × 2 μm and the data scale is 10 nm.

from 15.5 to 3.9 μA/cm^2 after 70 min thermal treatment. It is worthy to notice that the dark current of the annealed device (0.05 μA/cm^2 after 70 min thermal treatment) is larger than that of the as-prepared device (0.02 μA/cm^2), leading to a smaller signal-to-noise ratio. This phenomenon can also be found when 365 nm light is applied (Fig. 8b). The result is quite different from the previous reports describing the positive effect of thermal treatment on solar cell performance. For example, Clarke reported an over two times increase in short circuit current (J_{SC}) and photovoltaic device efficiency after thermal annealing [31]. Therefore, we further investigated this abnormal behavior in terms of morphology evolution below.

Since the PL spectra can shed light on the nature of the thin films, the aggregation of polymer chains after thermal annealing was investigated using the PL spectra [32]. Fig. 9a gives the annealing-induced PL spectral changes of the hybrid film containing 50 wt% TiO_2 nanocrystals. The annealing process was carried out in the vacuum, so the changes in fluorescence are independent of the oxygen-related structure changes in the polymer component. For the PL spectra of the as-prepared PFH and the hybrid films, there are two peaks centered at 425 and 447 nm. After annealing, the peaks are red-shifted by 5 nm, which is believed to be caused by the thermal-induced physical aggregation [33]. Furthermore, a significant quenching of the emission intensity occurs with the addition of TiO_2 nanocrystals and the quenching efficiencies are 55% and 28% for the as-prepared and the annealed hybrid films, respectively. The PL quenching is due to the exciton migration and relaxation through excimers, as reported previously [34]. Fig. 9b shows the UV–vis absorption changes before and after thermal treatment. The absorption spectra of the pure PFH and the hybrid film show the peak at 383 nm which is attributed to PFH. It is seen that the annealing broadens the absorption spectra. The spectral broadening is also attributed to the polymer aggregation [35].

In order to observe the morphology evolution more clearly, AFM was applied to monitor the morphology evolution of the hybrid films during the period of annealing. The results are shown in Fig. 10(a–e). For the as-prepared film, the surface is very smooth with r_{RMS} of 1.22 nm. The surface roughness increases with increasing the annealing time. For the sample annealed exceeding 40 min, a large extent of aggregation was observed with r_{RMS} of 1.52 nm. For the as-prepared film, the low extent of surface roughness effectively reduces the charge transport distance by forming large interfacial area between the two components and thus increases the current density [36]. For the reduced interfacial area after annealing, the exciton needs to travel longer distance to reach the donor/acceptor interface and has more chance to be radiatively relaxed, which is soundly supported by the PL spectra in Fig. 9. That is, the reduced interfacial area after annealing results in the decrease of the exciton dissociation efficiency as well as the photocurrent [37]. This means that the performance of the device is largely affected by a favorable morphology in the TiO_2/PFH system.

4. Conclusions

In summary, we have demonstrated a novel UV-A photodetector based on monodispersed OA-capped TiO_2 nanocrystals/polyfluorene hybrid material by a simple solution method. The obtained device shows high ultraviolet signal-to-noise ratio as well as fast response time of 200 ms under either UV irradiation or 365 nm light. Moreover, it exhibits linear dependence of light intensity on the photocurrent. According to the spectral response, the device shows high photosensitivity in the UV-A range with a peak

centered at 370 nm, indicating that the polymer PFH dominates the photoresponse of the hybrids. The thermal treatment is found to have no positive effect on the device performance. The proposed method is cost effective and amenable to large-scale production. These devices can show high performance for environmental and biological applications.

Acknowledgments

The work was financially supported by the NSFC (Grant Nos. 50773067, 50520150165, 51011130028 and 50990063). The authors also would like to thank the developing program of Changjiang Scholar and Innovation Team from Ministry of Education of China (Grant No IRT0651).

References

[1] Monroy E, Omnes F, Calle F. Semicond Sci Technol 2003;18(4):R33–51.
[2] Goldberg YA. Semicond Sci Technol 1999;14(7):R41–60.
[3] Averine SV, Kuznetzov PI, Zhitov VA, Alkeev NV. Solid-State Electron 2008;52 (5):618–24.
[4] Fang XS, Bando Y, Liao MY, Gautam UK, Zhi CY, Dierre B, et al. Adv Mater 2009;21(20):2034–9.
[5] Lee ML, Sheu JK, Lai WC, Su YK, Chang SJ, Kao CJ, et al. J Appl Phys 2003;94 (3):1753–7.
[6] Wang WS, Wu TT, Chou TH, Chen YY. Nanotechnology 2009;20(13):135503.
[7] Kong XZ, Liu CX, Dong W, Zhang XD, Tao C, Shen L, et al. Appl Phys Lett 2009;94(12):123502.
[8] Xue HL, Kong XZ, Liu ZR, Liu CX, Zhou JR, Chen WY. Appl Phys Lett 2007;90 (20):201118.
[9] Ray D, Narasimhan KL. Appl Phys Lett 2007;91(9):093516.
[10] Sandvik P, Brown D, Fedison J, Matocha K, Krechmer J. J Electrochem Soc 2005;152(3):G199–202.
[11] Lin HW, Ku SY, Su HC, Huang CW, Lin YT, Wong KT, et al. Adv Mater 2005;17 (20):2489–93.
[12] Wang MQ, Wang XG. Polymer 2008;49(6):1587–93.
[13] Zou LJ, Roddecha S, Anthamatten M. Polymer 2009;50(14):3136–44.
[14] Graziola F, Girardi F, Bauer M, Maggio RD, Rovezzi M, Bertagnolli H, et al. Polymer 2008;49(20):4332–43.
[15] Lin YY, Chen CW, Yen WC, Su WF, Ku CH, Wu JJ. Appl Phys Lett 2008;92 (23):233301.
[16] Yamaura J, Muraoka Y, Yamauchi T, Muramatsu T, Hiroi Z. Appl Phys Lett 2003;83(11):2097–9.
[17] Pan DC, Zhao NN, Wang Q, Jiang SC, Ji XL, An LJ. Adv Mater 2005;17 (16):1991–5.
[18] Wang ZJ, Qu SC, Zeng XB, Zhang CS, Shi MJ, Tan FR, et al. Polymer 2008;49 (21):4647–51.
[19] Wang W, Lin Y, Sun YP. Polymer 2005;46(20):8634–40.
[20] Li XL, Peng Q, Yi JX, Wang X, Li YD. Chem Eur J 2006;12(8):2383–91.
[21] Paronyan TM, Kechiantz AM, Lin MC. Nanotechnology 2008;19(11):115201.
[22] Chen RX, Maclaughlin S, Botton G, Zhu SP. Polymer 2009;50(18):4293–8.
[23] Huang YC, Liao YC, Li SS, Wu MC, Chen CW, Su WF. Sol Energy Mater Sol Cells 2009;93(6–7):888–92.
[24] Lin YT, Zeng TW, Lai WZ, Chen CW, Lin YY, Chang YS, et al. Nanotechnology 2006;17(23):5781–5.
[25] Li YB, Valle FD, Simonnet M, Yamada I, Delaunay JJ. Nanotechnology 2009;20 (4):045501.
[26] Su ZS, Li WL, Chu B, Li TL, Zhu JZ, Zhang G, et al. Appl Phys Lett 2008;93 (10):103309.
[27] Chang YM, Su WF, Wang L. Macromol Rapid Commun 2008;29(15):1303–8.
[28] Padinger F, Rittberger RS, Sariciftci NS. Adv Funct Mater 2003;13(1):85–8.
[29] Camaioni N, Ridolfi G, Casalbore-Miceli G, Possamai G, Maggini M. Adv Mater 2002;14(23):1735–8.
[30] Chang YM, Wang L. J Phys Chem C 2008;112(45):17716–20.
[31] Clarke TM, Ballantyne AM, Nelson J, Bradley DDC, Durrant JR. Adv Funct Mater 2008;18(24):4029–35.
[32] Jin H, Hou YB, Teng F, Kopola P, Tuomikoski M, Maaninen A. Sol Energy Mater Sol Cells 2009;93(2):289–94.
[33] Kim H, So WW, Moon SJ. Sol Energy Mater Sol Cells 2007;91(7):581–7.
[34] Salafsky JS. Phys Rev B 1999;59(16):10885–94.
[35] Zeng G, Yu WL, Chua SJ, Huang W. Macromolecules 2002;35(18):6907–14.
[36] Li G, Shrotriya V, Huang J, Yao Y, Emery K, Yang Y. Nat Mater 2005;4 (11):864–8.
[37] Zoombelt AP, Leenen MAM, Fonrodona M, Nicolas Y, Wienk MM, Janssen RAJ. Polymer 2009;50(19):4564–70.